7-20-2012

Characterization of $Ba_{1-x-y}Ca_xSr_yTiO_3$ Perovskites as Pb-Free Dielectric Materials

Lingling Zhang
University of South Carolina - Columbia, zhang257@email.sc.edu

Siwei Wang

Xusheng Wang

Kevin Huang
University of South Carolina - Columbia, huang46@cec.sc.edu

Publication Info

Published in *ECS Journal of Solid State Science and Technology*, Volume 1, Issue 2, 2012, pages N29-N32.

Publisher's Version: http://dx.doi.orgg/10.1149/2.019202jss
Zhang, Z., Wang, S., Wang, X., & Huang, K. (2012). Characterization of $Ba_{1-x-y}Ca_xSr_yTiO_3$ Perovskites as Pb-Free Dielectric Materials. ECS Journal of Solid State Science and Technology, 1 (2), N29 - N32. http://dx.doi.org/10.1149/2.019202jss

ECS Journal of Solid State Science and Technology, **1** (2) N29-N32 (2012)
2162-8769/2012/1(2)/N29/4/$28.00 © The Electrochemical Society

Characterization of $Ba_{1-x-y}Ca_xSr_yTiO_3$ Perovskites as Pb-Free Dielectric Materials

Lingling Zhang,[a,z] Siwei Wang,[a] Xusheng Wang,[b] and Kevin Huang[a,*,z]

[a]*Department of Mechanical Engineering, University of South Carolina, Columbia, South Carolina 29208, USA*
[b]*Functional Materials Research Laboratory, Tongji University, Shanghai 200092, China*

Use of lead-containing piezoelectric components in electrical and electronic devices has been banned on the EU market since July 1st, 2006. Development of lead-free high performance piezoelectric materials to meet the strong market demand is therefore imperative. In this paper, we report a systematic study on the structural, dielectric and ferroelectric properties of one class of lead-free piezoelectric materials, $Ba_{1-x-y}Ca_xSr_yTiO_3$ (x = 0-0.4, and y = 0-0.2) ceramics, using techniques such as XRD, SEM, impedance analyzer, and ferroelectric analyzer. It is found that with increasing Sr concentration in $Ba_{1-y}Sr_yTiO_3$ and $Ba_{0.8-y}Sr_yCa_{0.2}TiO_3$, the crystal structure transforms from tetragonal to cubic along with a decreased unit-cell volume. The microstructures of all samples prepared are uniform and dense with the grain size decreasing with Sr content. The Curie temperature decreases faster with Sr and Ca co-doped $BaTiO_3$ than that of Sr or Ca singularly-doped one. Above Curie temperature, a tunability of 31.4% can be achieved at an applied voltage of 30 kV/cm for ($Ba_{0.6}Ca_{0.2}Sr_{0.2}TiO_3$). These properties promise $Ba_{1-x-y}Ca_xSr_yTiO_3$ system to be applicable in Pb-free tunable devices.
 [DOI: 10.1149/2.019202jss]

Manuscript submitted April 24, 2012; revised manuscript received May 30, 2012. Published July 20, 2012.

Piezoelectric materials have broad applications in electronics, optics, sensors and actuators because of their excellent piezoelectric, pyroelectric, electro-optic and dielectric properties when applied in different fields.[1–4] Most of the commercially available high performance piezoelectric materials nowadays, however, contain high level of lead due to their excellent piezoelectric and ferroelectric properties arising from the unique crystal chemistry of Pb^{2+} ion. $PbTiO_3$ (PT) and $Pb(Zr_xTi_{1-x})O_3$ (PZT) have been the most commercially available ferroelectric systems for more than half a century. Other Pb-containing complex pervoskites, e. g., $Pb(Mg_{1/3}Nb_{2/3})O_3$ (PMN), $Pb_{1-x}La_x(Zr_{1-y}Ti_y)_{1-x/4}O_3$ (PLZT), $Pb_{1-x}Sr_x(Zr_{1-y}Ti_y)_{1-x/4}O_3$ (PSZT) have also been extensively studied.[5] However, a long-term exposure of Pb to human beings at higher than permitted level can cause severe health problems. Effective on July 1 2006, the Restriction on the Use of Hazardous Substances or RoHS Directive officially bans sales on the EU market of any new electrical and electronic equipment containing lead higher than the required levels.[6] Therefore, lead-free piezoelectric materials with high performance are in great demand. Among the lead-free piezoelectric materials, $ATiO_3$-based (A=Ba, Sr, Ca),[7–12] (K,Na)NbO_3-based[12–15] and bismuth layer structured ferroelectrics (BLSF).[12,16] ceramic materials have gained much renewed attention in recent years. $ATiO_3$-based perovskites stand out to be the most promising lead-free piezoelectric/dielectric materials.

$BaTiO_3$ is a class of ferroelectric materials that have been actively studied since 1950s.[17,18] It exhibits a phase transition from cubic (paraelectric) to tetragonal (ferroelectric) at 120°C. In contrast, $SrTiO_3$ and $CaTiO_3$ belong to quantum paraelectrics and undergo no ferroelectric phase transition.[17,19] The binary system (1-x)$BaTiO_3$-$x$$SrTiO_3$ and (1-x)$CaTiO_3$-$x$$SrTiO_3$ are both congruent solid solutions over the entire x range. The former is a ferroelectric material whose Curie temperature T_c decreases with Sr concentration, and has been extensively studied due to its high dielectric constant and interesting relaxor ferroelectric behavior.[3–5,20] The latter has been applied as a dielectric component in microwaves.[21,22] The increase in Sr concentration in (1-x)$BaTiO_3$-$x$$SrTiO_3$ leads to an almost linear decrease in T_c (T_c(K) = 360x + 45, x = 0.15-1.0),[21] which is caused by the decrease in the unit cell volume of the perovskite structure. In our previous study, (1-x)$BaTiO_3$-$x$$CaTiO_3$ was shown to form a complete solid solution at x<0.24 with a negligible change in T_c.[23,24] While the Ca^{2+} has a smaller ionic radius than Ba^{2+}, Ca^{2+} exhibits a greater atomic polarizability. This intensifies the interactions between the Ti-ions, which compensates for the decrease in T_c originated from the shrinkage of the unit cell volume by the Ca-doping.[17,25] Another interesting phenomenon is that a small fraction of Ca^{2+} can substitute the Ti-ions on the B-site in (1-x)$BaTiO_3$-$x$$CaTiO_3$ provided that the molar ratio of (Ba+Ca)/Ti = 1.[26]

The intriguing features induced by the Ca- and Sr co-doping in $BaTiO_3$-based materials make the $BaTiO_3$-$CaTiO_3$-$SrTiO_3$ (BSCT) a very attractive candidate for both theoretical and experimental investigations. Curie temperature is a characteristic of ferroelectric materials, the magnitude of which determines the real operation of ferroelectric devices. Therefore, a scientific understanding of Curie temperature and its underlying ferroelectric behavior can underpin the development of new high-performance dielectric materials. Although a great deal of works has been reported in recent years, a more systematic investigation is still lacking. In this paper, we report a systematic study on the effects of Ca and Sr co-doping on the curie temperatures and dielectric properties of the BSCT system.

Experimental

The phase diagram of the ternary system $BaTiO_3$ (BT)-$CaTiO_3$ (CT)-$SrTiO_3$ (ST) reported earlier[27] is shown in Figure 1. Our compositions were selected in the Ba-rich region. The ceramics were synthesized by solid state reaction according to the stoichiometric composition of $Ba_{1-x-y}Sr_yCa_xTiO_3$ located on the broken lines: (1) y = 0, x = 0-0.4; (2) y = 0.05, x = 0-0.4; (3) y = 0.1, x = 0-0.4; (4) y = 0.13, x = 0-0.4; and (5) y = 0.20, x = 0-0.4. Raw materials of $BaTiO_3$ and $SrTiO_3$ (99.9%, hydrothermally synthesized by Shandong Guoteng Materials Co. Ltd.), $CaCO_3$ (99.99%, Sinopharm Chemical Reagent Co. Ltd.), and TiO_2 (99.9%, Nanhai High-Tech Inorganic Materials Co. Ltd), were first mixed with assistance of alcohol, then dried and heated in air at 900°C for 4 hrs. Thereafter, the pre-calcined powders were pulverized, intimately mixed with 8 wt% polyvinyl alcohol as binder and pressed into 10-mm in diameter pellets and sintered in air at 1400°C for 4 h. All samples had a density greater than 93% of the theoretical values.

The sample crystallinity was examined with an X-ray diffractometer (XRD, D8 Advance, Bruker AXS GmbH) and a scanning electron microscopy (SEM, JSM-5510, JEOL). The thickness of sintered pellets were first reduced to about 1.0 mm for normal dielectric measurements, then to 0.5 mm for Polarization-Field (P-E) loops measurements, and finally to 0.3 mm for bias field dependence measurements,. For electrical measurements, silver electrodes were applied to both surfaces of the specimens. Dielectric properties were characterized using a high-precision LCR meter (HP 4284A, Hewlett Packard) in a temperature-controlled chamber. P-E and Strain-Field (S-E) loops were measured by a precision ferroelectric/piezoelectric analyzer (Premier ll, Radiant Technologies Inc.). Bias field dependence measurements were carried out using an automated home-made

*Electrochemical Society Active Member.
[z]E-mail: zhang257@email.sc.edu; kevin.huang@sc.edu

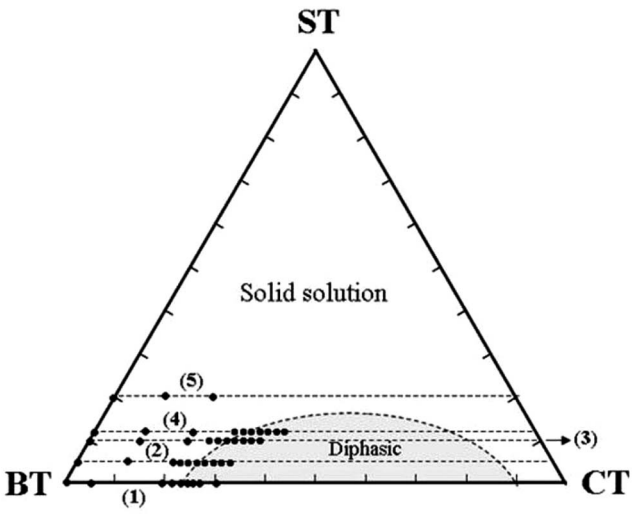

Figure 1. Phase diagram of the ternary system (1-*x*-*y*)$BaTiO_3$ (BT)-*x*$CaTiO_3$ (CT)-*y*$SrTiO_3$ (ST)[26] showing compositions investigated: (1) $y = 0$; (2) $y = 0.05$; (3) $y = 0.1$; (4) $y = 0.13$; and (5) $y = 0.20$. Inset:

ε-E analyzer system including an LCR meter, a high-voltage generator and a sample chamber.

Results and Discussion

Phase evolution and microstructures.— The X-ray diffraction patterns of the $Ba_{1-y}Sr_yTiO_3$ (BST) (y = 0, 0.13, 0.20) ceramics and $Ba_{0.8-y}Sr_yCa_{0.2}TiO_3$ (BSC20T) ($y = 0$, 0.13, 0.20) sintered at 1400°C are shown in Figs. 2a and 2b, respectively. It is evident that all the ceramics have a well crystallized perovskite structure without impurity phases. To closely examine the peak positions and splitting of samples with different compositions, the step-scanned refined X-ray patterns located at $2\theta = 31$ to 33° and 44 to 46°, representing (110), (002) and (200) planes, are shown in the insets of the figures. With increasing Sr content, the tetragonal (110) peak of BST and BSC20T shifts to a higher 2θ angle, suggesting that the lattice constant decreases with Sr. Since the ionic radius of Sr^{2+} (1.44 Å) is smaller than that of Ba^{2+} (1.61 Å),[28] the reduced lattice constant suggests that Sr^{2+} enter A-sites of the perovskite structure by replacing Ba^{2+}, which was also confirmed by Krishna et al.[26] The refined XRD patterns of $BaTiO_3$ and $Ba_{0.87}Sr_{0.13}TiO_3$ show split reflections at (200) and (002) peaks, indicating a tetragonal symmetry for both samples. On the other hand, the XRD patterns of $Ba_{0.8}Sr_{0.2}TiO_3$ and $Ba_{0.67}Sr_{0.13}Ca_{0.20}TiO_3$ have a single reflection at (200) peak showing a cubic symmetry. From the split reflections, it is concluded that the BST and BSC20T transform from tetragonal to cubic as Sr concentration increases.

Morphological analysis on grains and grain boundaries of the BSCT was carried out with SEM. Taking BSC20T as an example, the surface SEM micrograph is shown in Fig. 3. It reveals a dense microstructure with an average grain size decreasing from 18.3 μm (Fig. 3a) to 5.2 μm (Fig. 3c) with increase in Sr concentration. It is well known that the grain size is strongly influenced by the rate of nucleation N and the rate of the grain growth G. If N is greater than G, the final grain size would be small. Both rates depend heavily on the composition and temperature.[29] In our study, the decrease of grain size forBSC20T is mainly caused by the increased nucleation rate due to the composition change induced by the presence of Sr.[30]

Electrical properties.— The electric properties of BSCT as a function of Ca concentration are presented as follows. The variations of dielectric constant measured at 10 kHz with temperature ranging from −150 to 150°C are shown in Figure 4 for (a) $Ba_{1-x}Ca_xTiO_3$, (b) $Ba_{0.95-x}Sr_{0.05}Ca_xTiO_3$ (BS5CT), (c) $Ba_{0.9-x}Sr_{0.1}Ca_xTiO_3$ (BS10CT), (d) $Ba_{0.87-x}Sr_{0.13}Ca_xTiO_3$ (BS13CT), and (e) $Ba_{0.80-x}Sr_{0.20}Ca_xTiO_3$

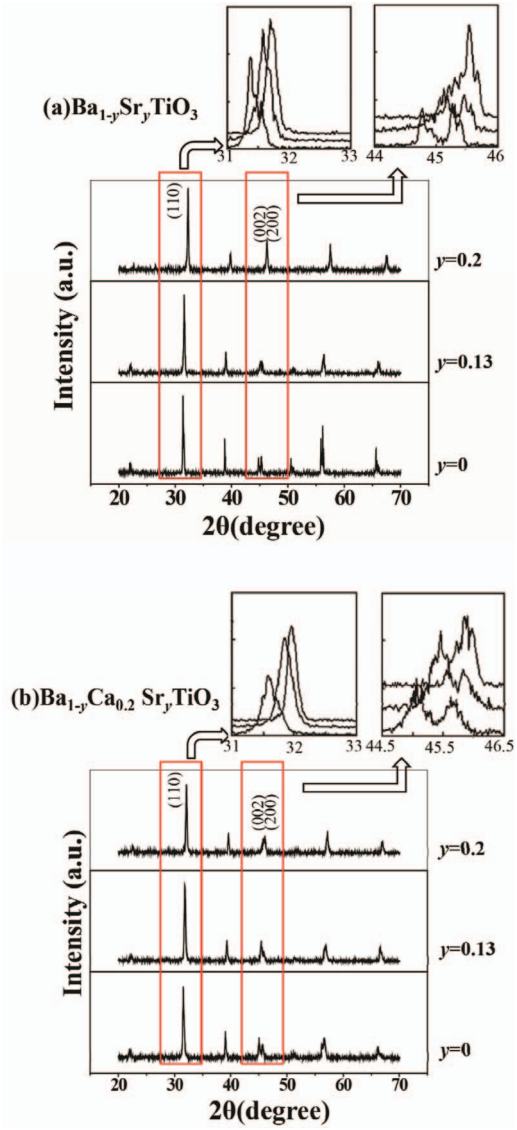

Figure 2. XRD pattern of $Ba_{1-y}Sr_yTiO_3$ (y = 0, 0.13, 0.20) ceramics and $Ba_{0.8-y}Ca_{0.2}Sr_yTiO_3$ (y = 0, 0.13, 0.20) sintered at 1400°C.

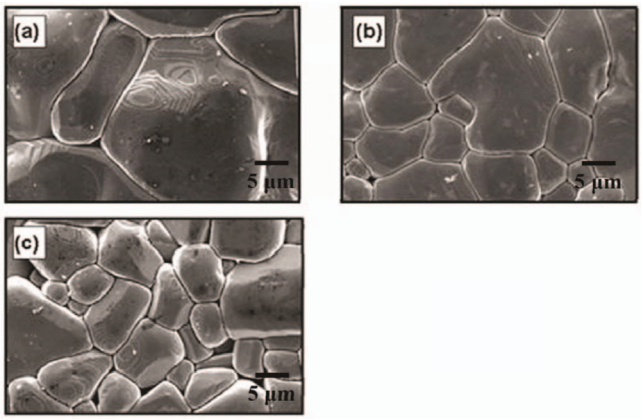

Figure 3. SEM micrographs of $Ba_{0.8-y}Ca_{0.2}Sr_yTiO_3$ for $y = 0$, 0.13, and 0.20 samples.

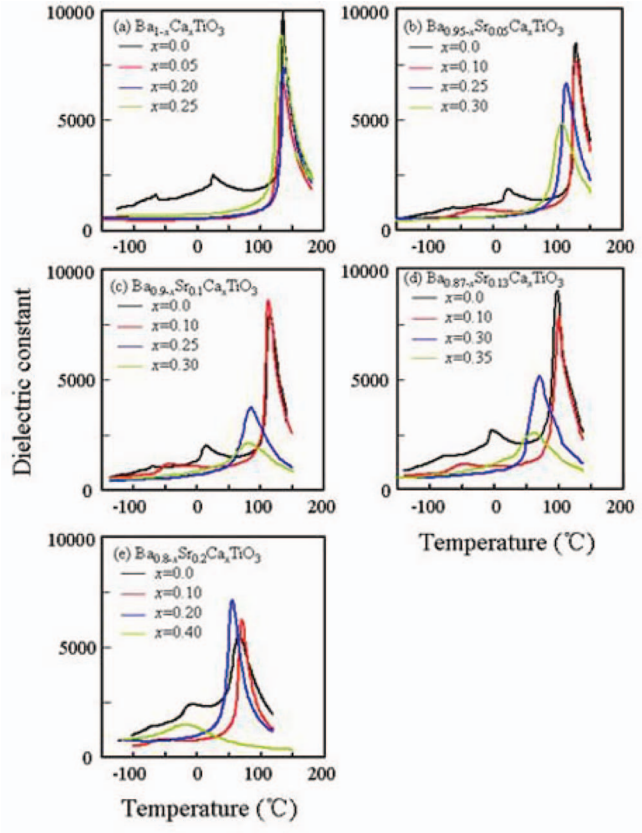

Figure 4. Variations of the dielectric constant of $Ba_{1-x-y}Sr_yCa_xTiO_3$ (x = 0-0.40, y = 0-0.20) ceramics with temperature at frequency of 10 kHz.

(BS20CT), respectively. It is evident from Fig. 4a that the curve remains fairly flat before ~120°C for samples with Ca concentrations falling into the solid solution region. After the Curie temperature (T_c), the dielectric peaks decrease in height and become broadened. Similarly, the dielectric constants of BS5CT (Fig. 4b), BS10CT (Fig. 4c), BS13CT (Fig. 4d), and BS20CT (Fig. 4e) have the same trend with increasing Ca concentration.

For a better understanding of what is observed in Fig. 4, the relationship between T_c and Ca content x is plotted in Figure 5 for

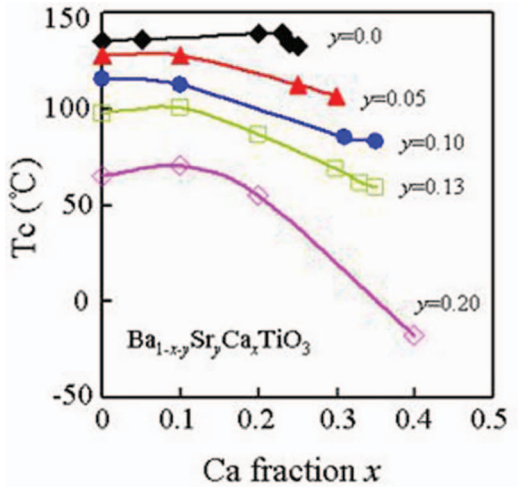

Figure 5. T_c vs Ca fraction x in $Ba_{1-x-y}Sr_yCa_xTiO_3$ (x = 0-0.40, y = 0-0.20) ceramics at frequency of 10 kHz.

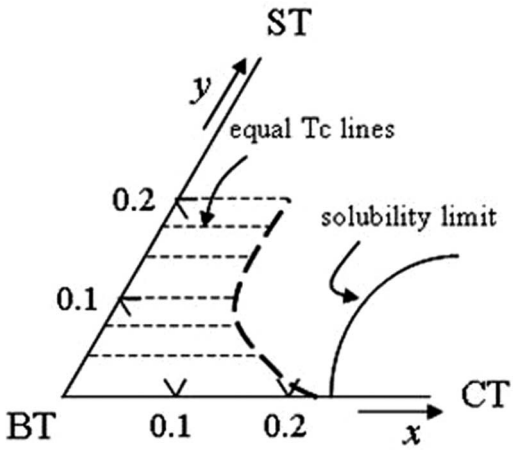

Figure 6. Partial phase diagram of the ternary system $BaTiO_3$-$CaTiO_3$-$SrTiO_3$ showing the equal T_c lines and the solubility limit.

$Ba_{1-x-y}Sr_yCa_xTiO_3$ (x = 0-0.40, y = 0-0.20) measured at 10 kHz. Since the ionic radius for Ca^{2+} (1.34 Å) is smaller than Sr^{2+} and Ba^{2+},[28] one may expect that T_c decreases with x, similar to the Sr effect observed in (1-x)$BaTiO_3$-$x$$SrTiO_3$ (T_c(K) = 360x + 45, x = 0.15-1.0).[22] What is unexpected is that the T_c remains relatively constant at lower x. The underlying reason could be the higher atomic polarizability owned by Ca^{2+}.[17] This would intensify the interaction between Ti-ions and stabilize or slightly increase the T_c as is in the system $Pb_xBa_{1-x}TiO_3$ where the T_c increases with Pb concentration.[31] Upon further increasing x, the decreased unit-cell volume offsets the polarizability effect induced by Ca^{2+}, leading to a decrease in T_c. By substituting Ca^{2+} into Sr^{2+} or Ba^{2+}, the bonding between the A-site ions and O^{2-} in the ABO_3 structure becomes stronger because the smaller Ca^{2+} brings about a decrease in the c/a ratio (the ratio of the a-axis lattice parameter and c-axis lattice parameter), thus inducing a drop in T_c.

In order to clearly elucidate the relationships of T_c with Ca, Sr and Ba contents, we introduce equal T_c line into the ternary phase diagram. The equal T_c line and solubility limit (as discussed in our previous investigations[32]) are shown as a part of the ternary phase diagram of BCST system in Fig. 6. It is evident that the T_c decreases faster with Sr and Ca in co-coped $BaTiO_3$ than that in Sr or Ca doped one when Ca concentration exceeds the equal T_c line. Two possible reasons could interpret the shape of the equal T_c line. First, in the areas outside the equal T_c line, the marked shrinkage of the unit-cell volume offsets the polarizability effect caused by Ca^{2+}. This results in a reduction in the lattice constant, which in turn elevates the lattice stresses and therefore forces the T_c to move downward. This is also the reason why the T_c of $BaTiO_3$ decreases faster when co-doped with Sr and Ca than that with Sr-single dopant. Second, as aforementioned, the binary system (1-y)$BaTiO_3$-$y$$SrTiO_3$ forms a congruent solid solution throughout the x range whereas (1-x)$BaTiO_3$-$x$$CaTiO_3$ has a solubility in the range of x = 0 to 0.25 and of x = 0.90 to 1. It seems to be reasonable to postulate that Sr^{2+} enters preferentially into the Ba-site, forcing more Ca^{2+} to enter Ti-site. Since the ionic radius of Ca^{2+} is larger than that of Ti^{4+}, Ca^{2+}-replacement of Ti^{4+} in the octahedral sites of the perovskite structure will result in a localized expansion of the unit cell, which further compresses the nearest neighbor unit cells.[33] Ca^{2+} substitution for Ti^{4+} impedes the ferroelectric distortion of the TiO_6 octahedral of the neighboring unit cells, which causes a more pronounced decrease of T_c in Sr and Ca co-doped $BaTiO_3$ than Ca-doped one when Ca concentration falls outside the equal T_c line shown in Figure 6.

To reveal the ferroelectric feature of the BSCT ceramics, the P-E field hysteresis loops and electrostrictive S-E field butterfly curves for various Ca concentrations are shown in Fig. 7. Because these five series samples have the same characteristic, we take $Ba_{0.8-x}Sr_{0.20}Ca_xTiO_3$

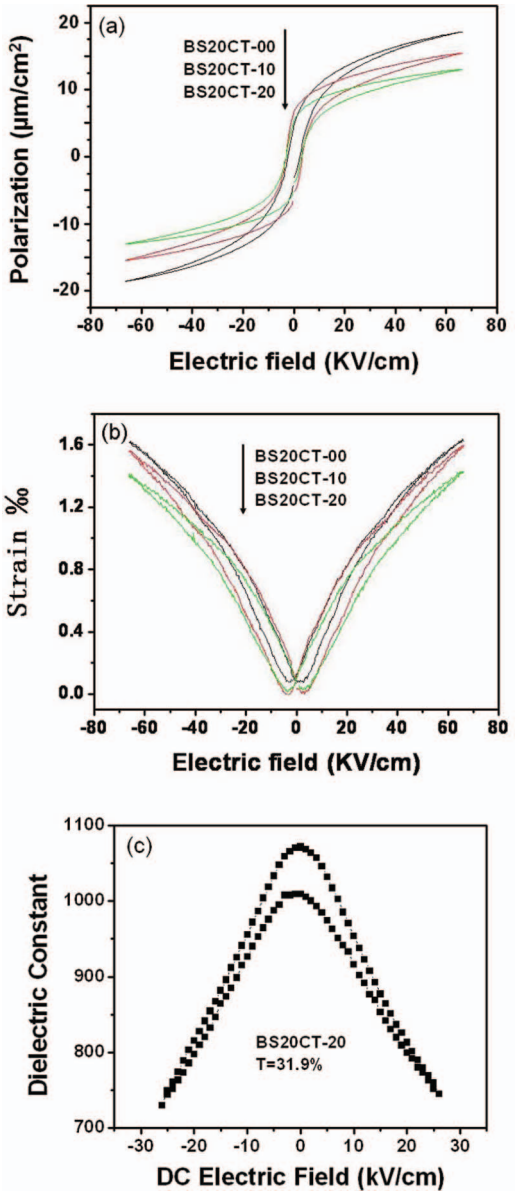

Figure 7. (a) Polarization vs electric field and (b) Electric-field-induced strain-electric field butterfly curves for $Ba_{0.8-x}Sr_{0.20}Ca_xTiO_3$ (x = 0, 0.10 and 0.20) ceramics; (c) The dielectric constant-electric field (ε-E) relation of $Ba_{0.6}Sr_{0.2}Ca_{0.2}TiO_3$ sample at room temperature and 10 kHz.

as an example to show in Figure 7 with (a) polarization vs electric field and (b) electric-field-induced strain-electric field butterfly curves. Under an applied electric field of 70 kV/cm, the polarization-electric field hysteresis loops are flattened and the remnant polarization decreases with increase x. For samples of x = 0, 0.10, and 0.20, the remnant polarization values are 18, 15 and 13 μC/cm^2 and electrostrictive strain values are about 0.16, 0.156 and 0.14% at ±70 kV/cm driving field, respectively. The curves show the expected hysteresis behavior because of the ferroelectric nature. With increasing Ca concentration, the remnant polarization decreases due to the presence of the cubic paraelectric phase. Even though the remnant polarization and electrostrictive strain decrease with increasing Ca content, the tunability value reaches 31.4% at an applied voltage of 30 kV/cm and frequency of 10 kHz, see Fig. 7c. The high tunability of the material, which indicates the ability of dielectric constant can be changed in a larger scale versus applied voltage, implies the material is of potential for the application of tunable devices.

Conclusions

The powder XRD patterns show the diffraction peaks of BST and BS20CT ceramics systematically shift toward higher 2θ with increasing Sr, an indication of Sr^{2+} entering A-site and shrinking the unit cell. The merge of peaks (002) and (200) suggests that the phase transformation occurs from tetragonal to cubic. All samples are uniform and dense in microstructure, and the grain sizes decrease with increasing Sr concentration. The Curie temperature T_c is found to decrease faster in Sr and Ca co-doped $BaTiO_3$ than in Sr or Ca singularly doped one. Above T_c, a large value of tunability is obtained around 31.4% at an applied voltage of 30 kV/cm. The unique effect of co-doping in A-site on the dielectric properties for $BaTiO_3$ based ferroelectric/ piezoelectric materials will find practical applications.

Acknowledgments

This work was supported by the Natural Science Foundation of China (No. 50932007), Foundation of Doctor Training Program in University and College in China (No. 20070247010) and Scientific and Technological Innovation Program of Shanghai (No. 08JC1419100).

References

1. M. E. Lines and A. M. Glass, *Principles and Applications of Ferroelectrics and Related Materials*, Clarendon Press, Oxford (1977); Y. Xu, *Ferroelectric Materials and Their Applications*, Elsevier Press, Amsterdam (1991).
2. K. Uchino, *Piezoelectric Actuators and Ultrasonic Motors*, Kluwer Academic, Boston (1997).
3. N. Setter and R. Waser, *Acta Mater.*, **48**, 151 (2000).
4. A. K. Tagantsev, V. O. Sherman, K. F. Astafiev, J. Venkatesh, and N. Setter, *J. Electroceram.*, **11**, 5 (2003).
5. G. H. Haertling, *J. Am. Ceram. Soc.*, **82**, 797 (1999).
6. See http://www.rohs.eu/english/index.html for the RoHS regulation (Directive 2002/95/EC).
7. S. Wang, J. Zhai, X. Chou, L. Zhang, and X. Yao, *Mater. Chem. Phys.*, **115**, 200 (2009).
8. X. Ren, *Nat. Mater.*, **3**, 91 (2004).
9. D. Fu, M. Itoh, S. Koshihara, T. Kosugi, and S. Tsuneyuki, *Phys. Rev. Lett.*, **100**, 227601 (2008).
10. C. Ang, Z. Yu, Z. Jing, R. Guo, A. S. Bhalla, and L. E. Cross, *Appl. Phys. Lett.*, **80**, 3424 (2002).
11. S. T. Zhang, A. B. Kounga, E. Aulbach, T. Granzow, W. Jo, H. J. Kleebe, and J. Rödel, *J. Appl. Phys.*, **103**, 034107 (2008).
12. T. Takenaka, H. Nagata, and Y. Hiruma, *Jpn. J. Appl. Phys.*, **47**, 3787 (2008).
13. Y. Saito, H. Takao, T. Tani, T. Nonoyama, K. Takatori, T. Homma, T. Nagaya, and M. Nakamura, *Nature (London)*, **84**, 432 (2004).
14. S. Zhang, R. Xia, and T. R. Shrout, *Appl. Phys. Lett.*, **91**, 132913 (2007).
15. J. Wu, D. Xiao, Y. Wang, J. Zhu, L. Wu, and Y. Jiang, *Appl. Phys. Lett.*, **91**, 252907 (2007).
16. T. Takenaka and H. Nagata, *Ferroelectrics*, **336**, 119 (2006).
17. T. Mitsui and W. B. Westphal, *Phys. Rev.*, **124**, 1354 (1961).
18. B. Jaffe, W. R. Cook, and H. Jaffe, *Piezoelectric Ceramics*, Academic Press, London (1971).
19. K. A. Muller and H. Burkard, *Phys. Rev. B*, **19**, 3593 (1979).
20. J. H. Jeon, *J. Euro. Ceram. Soc.*, **24**, 1045 (2004).
21. V. V. Lemanov, *Phys. Solid State*, **39**, 1468 (1997).
22. P. L. Wise, I. M. Reaney, W. E. Lee, T. J. Price, D. M. Iddles, and D. S. Cannell, *J. Euro. Ceram. Soc.*, **21**, 2629 (2001).
23. X. Wang, H. Yamada, and C. N. Xu, *Appl. Phys. Lett.*, **86**, 022905 (2005).
24. X. Wang, L. Zhang, H. Liu, J. Zhai, and X. Yao, *Mater. Chem. Phys.*, **112**, 675 (2008).
25. X. R. Cheng and M. R. Shen, *Solid State Commun.*, **141**, 587 (2007).
26. P. S. R. Krishna, D. Pandey, V. S. Tiwari, R. Chakravarthy, and B. A. Dasannacharya, *Appl. Phys. Lett.*, **62**, 231 (1993).
27. M. Mcquarrie, *J. Am. Ceram. Soc.*, **38**, 444 (1955).
28. R. D. Shannon, *Acta Cryst.*, **A32**, 751 (1976).
29. D. Hennings, *Int. J. High Technol. Ceram.*, **3**, 91 (1987).
30. J. H. Yoo, W. Gao, and K. H. Yoon, *J. Mater. Sci.*, **34**, 5361 (1999).
31. G. Shirane and K. Suzuki, *J. Phys. Soc. Japan*, **6**, 274 (1951).
32. L. Zhang, X. Wang, H. Liu, and X. Yao, *J. Am. Ceram. Soc.*, **93**, 1049 (2010).
33. Z. Q. Zhuang, M. P. Harmer, D. M. Smyth, and R. E. Newnham, *MRS Bull.*, **22**, 1329 (1987).